Chin. Sci. Bull. (2014) 59(28):3676–3685
DOI 10.1007/s11434-014-0400-9

csb.scichina.com
www.springer.com/scp

Article

Engineering Thermophysics

Significant heat transfer enhancement for R123 condensation by micromembrane cylinder

Jian Xie · Feng Xing · Jinliang Xu · Huan Liu

Received: 17 December 2013 / Accepted: 24 February 2014 / Published online: 5 June 2014

Abstract Renewable energy or low grade energy utilizations need high performance of phase change heat exchangers. Suspending micromembrane cylinder in tube (called modulated heat transfer tube) increases the void fractions or vapor qualities near the tube wall to significantly enhance heat transfer. The R123 condensation heat transfer with horizontal position was investigated. The results for the bare tube and modulated heat transfer tube were tested case by case. It is found that the modulated heat transfer tube significantly enhance the condensation heat transfer, with the heat transfer enhancement factors (EF) covering the range of 1.118–2.124. The comprehensive performance evaluation criteria (PEC) had the range of 0.71–1.66, with most of runs behaving PEC larger than 1.0. For the two-phase outlet conditions, the EF values are increased with increases in the vapor mass fluxes, Gx_{in}, where G is the mass flux and x_{in} is the inlet vapor mass quality. The EF values are inversely related to Gx_{in} for the subcooled liquid outlet cases. The enhanced heat transfer mechanisms are analyzed with the observed images together with the discussion of pressure and velocity distributions.

Keywords Heat transfer enhancement · Micromembrane cylinder · Condensation

J. Xie · F. Xing · J. Xu (✉) · H. Liu
The Beijing Key Laboratory of Multiphase Flow and Heat Transfer, North China Electric Power University, Beijing 102206, China
e-mail: xjl@ncepu.edu.cn

1 Introduction

Fresh concept is necessary to extract thermal energy for the low grade or renewable energy utilizations. Due to the low temperature level of these heat sources, the conventional method to extract the thermal energy may cause unacceptable investment cost. For instance, a heat exchanger for an ocean thermal energy conversion (OTEC) plant requires a heat transfer surface area in the order of 10^4 m^2/MW [1]. Miniaturization of heat exchangers increases the system efficiencies and decreases the investment cost.

The waste heat driven refrigeration or heat pump systems are effective ways to recover the low grade heat [2, 3]. Expanding the waste heat utilization should decrease the component/system size and investment cost. The evaporator and condenser are necessary in these systems with organic fluids used instead of water. Organic fluids have lower specific heats, thermal conductivities and latent heat of evaporation compared with water. Thus, they are lower in the phase change heat transfer performance compared with water.

A hot research and development area is to use an Organic Rankine Cycle (ORC) to extract the low grade heat. Heat evaporates the organic liquid (such as R123) to generate vapor, driving the turbine to produce power. Then, a condenser shrinks the vapor mixture to liquid which is circulated by a pump. The improvement of the phase change heat transfer within the ORC system helps to decrease the energy destruction for the component and system and increase the power output.

Many studies existed in the open literature for the condensation heat transfer enhancement such as Graham et al. [4], Cavallini et al. [5], Miyara and Otsubo [6], Laohalertdecha and Wongwises [7], etc. Heat transfer enhancement mechanism is attributed by mixing the fluid

boundary layers and limiting the growth of fluid boundary layers close to the tube wall. The enhancement by the microstructures on the tube wall is beyond the scope of the present study.

Recently, our research group [8] tried to modify the flow patterns in a tube by the capillary separation effect. A micromembrane cylinder is suspended in the tube. Mesh pores prevent gas bubbles from entering the micromembrane cylinder but capture liquid into the micromembrane cylinder, increasing the void fractions near the tube wall and yielding thin liquid films on the wall. Then, we performed the numerical simulation of flow pattern modulations for the air-water vertical upflows [9]. The results do show that most of gas phase is flowing near the tube wall. Thus, the liquid film thickness on the wall is sharply decreased. This paper presented the preliminary experimental results for the modulated condensation heat transfer in a horizontal tube.

2 The micromembrane design and experimental setup

Figure 1a shows the micromembrane photo. The micromembrane cylinder consisted of two layers, having a plain weave mesh screen surface and a cylinder mesh screen surface. The two layers were welded together. The micromembrane cylinder had an outer diameter of 11.20 mm and a total length of 1,698 mm. Figure 1b, c shows the SEM pictures for the outer layer and inner layer, respectively. For the porous media, PPI refers to pores per inch. The outer layer of mesh screens had PPI of 200, having the rectangular cross section with the pore width of 76 μm and the mesh wire thickness of 46 μm. The inner layer of mesh screen acts as the supporting structure function. Thus, it had the PPI of 80 with the mesh pore width of 194 μm and the mesh wire thickness of 130 μm. When the micromembrane is wet, the gas-liquid interface curvature within the mesh pores generates large surface tension force to resist the gas phase entering the micromembrane cylinder. This will increase the gas (or vapor) void fractions in annular region between the micromembrane cylinder and the copper tube to enhance the heat transfer. Compared with the solid cylinder, the flow cross section area is less reduced thus the penalty of the pressure drop increment is smaller.

Figure 2 shows the experimental setup. The R123 liquid was stored in a reservoir. The organic fluid loop circulated the R123 fluid. A piston pump provided the R123 flow rate to the loop. A bypass line connected the pump inlet and outlet. An accumulator was installed at the pump outlet to stabilize the fluid pressure. The R123 flow rate was in the range of 0–100 kg/h and 0–1,000 kg/h. Then, the R123 liquid was evaporated in a helical-coiled tube to generate two-phase mixture. The inlet vapor mass quality of the test section was controlled by the heating power applied on the helical-coiled tube. The two-phase mixture was condensed in the horizontal test section. The cooling water flowing in the tube annulus was provided by a chiller machine. The inlet cooling water temperature was maintained to be 25 ± 0.3 °C. The cooling water flow rate was adjusted by the control valve and was measured by a mass flow mater in the range of 0–1,200 kg/h. The pressures and temperatures were measured by the pressure and temperature sensors, respectively. The pressure at the inlet of the test section was maintained to be 250 ± 5 kPa with the corresponding saturation temperature of 55 ± 0.5 °C. Two Pyrex glass tubes were arranged at the inlet and outlet of the test section to observe the flow patterns. The fluid at the outlet of the test section was further cooled by the tap-water and then returned to the liquid storage tank, which was immersed in a constant temperature bath to have the temperature of 10 ± 0.4 °C. The K-type jacket thermocouples measured the fluid temperatures with the accuracy

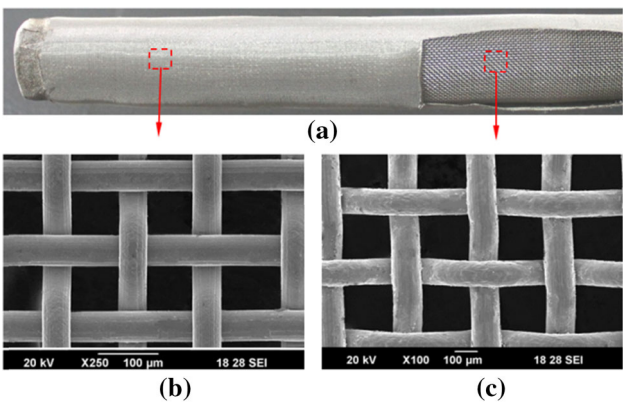

Fig. 1 (Color online) The photo of fabricated micromembrane cylinder (**a**), the outer layer of micromembrane cylinder (**b**) and the inner layer of micromembrane cylinder (**c**)

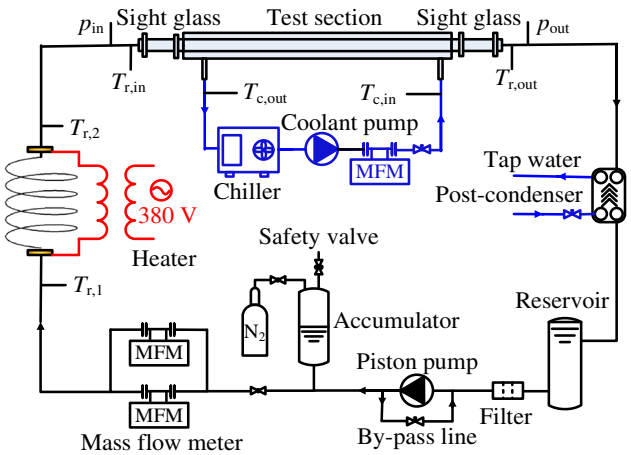

Fig. 2 (Color online) The experimental setup

of 0.2 °C. All the signals were collected by a data acquisition system.

Figure 3 shows the counter-current condenser test section, consisting of an inner copper tube and an outer stainless steel tube. The copper tube had an outer diameter of 18.97 mm with the thickness of 2.08 mm. It had an inner diameter of 14.81 mm, with the heat transfer length of 1200 mm. The 304 stainless steel tube had an inner diameter of 23.80 mm, forming a tube annulus of 2.41 mm. The R123 two-phase mixture was flowing in the copper tube while the cooling water was flowing in the tube annulus. A layer of thermal insulation material with a thickness of 5 cm was wrapped on the outer stainless tube to decrease the heat loss to the environment. Along the flow direction, thermocouples were arranged on the top, side and bottom locations of the tube for seven cross sections. Tests were performed inside the same copper tube with and without the micromembrane cylinder inserted. For the modulated heat transfer experiment, the two-phase stream attacks the side mesh screen surface. The inlet and outlet parts of the micromembrane cylinder were in the Pyrex glass tube so that the flow observation can be performed. Four supporting claws were arranged between the inner copper tube wall and the micromembrane cylinder to uniformly hold the micromembrane in the copper tube.

3 Data reduction and process

The parameters involved in the experiment are: the R123 mass flow rate m_r, the cooling water flow rate m_c, the temperature at the inlet of the helical-coiled tube $T_{r,1}$, the inlet temperature of the test section $T_{r,in}$, the outlet temperature of the test section $T_{r,out}$, the inlet pressure of the test section $P_{r,in}$, the outlet pressure of the test section $P_{r,out}$, the wall temperature over various cross sections $T_{i,t}$, the side wall temperature $T_{i,s}$, the bottom wall temperature $T_{i,b}$, the coiling water temperature $T_{i,c}$. $T_{c,out}$ and $T_{c,in}$ are the cooling water temperatures at the cross sections 1 and 7. The voltage applied on the helical-coiled tube was U and the current was I. Besides, the copper tube inside and outside diameters were d_i and d_o and the effective heat transfer length was L_e. The physical properties of R123 were cited from REFPROP version 8.0.

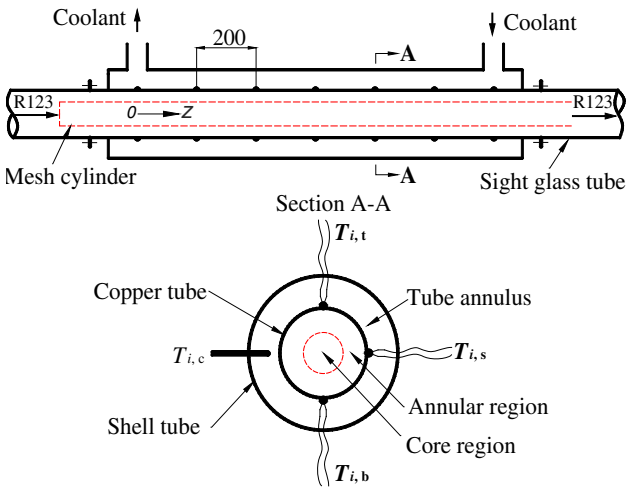

Fig. 3 (Color online) The test section

3.1 The inlet and outlet vapor mass qualities of the test section

The inlet vapor mass quality of the test section is

$$x_{in} = \frac{i_{r,1} + UI/m_r - i_{l,in}}{i_{v,in} - i_{l,in}}, \quad (1)$$

where $i_{r,1}$ is the enthalpy at the inlet of the helical-coiled tube, $i_{v,in}$ and $i_{l,in}$ are the saturated vapor and liquid enthalpies at the inlet of the test section, corresponding to the inlet pressure of $P_{r,in}$.

The heat transfer rate across the condenser test section is

$$Q = m_c C_{p,c}\left(T_{c,out} - T_{c,in}\right), \quad (2)$$

where $C_{p,c}$ is the cooling water specific heat determined by the average temperature of $T_{c,ave}$.

The outlet parameters of the test section can be decided based on the inlet parameters and the heat transfer rate across the condenser test section. The outlet vapor quality of the test section is

$$x_{out} = \frac{i_{r,in} - Q/m_r - i_{l,out}}{i_{v,out} - i_{l,out}}, \quad (3)$$

where the saturated vapor enthalpy $i_{v,out}$ and liquid enthalpy $i_{l,out}$ are determined based on the outlet pressure of $P_{r,out}$. If the outlet temperature $T_{r,out}$ of R123 is less than the saturation temperature corresponding to the outlet pressure $P_{r,out}$, the outlet vapor quality is negative.

3.2 R123 condensation heat transfer coefficient

Based on the thermal resistance analysis, the condensation heat transfer coefficient in the copper tube is [10]:

$$h = \frac{1}{\frac{1}{h_{total}} - \frac{d_i}{2k}\ln\left(\frac{d_o}{d_i}\right) - \frac{d_i}{d_o}\frac{1}{h_c}}. \quad (4)$$

In Eq. (4) the total heat transfer coefficient is the heat flux divided by the logarithm mean temperature difference (LMTD):

$$h_{total} = \frac{Q}{\pi d_i L_e \cdot \mathrm{LMTD}}. \quad (5)$$

The forced convective heat transfer coefficient of the cooling water in the tube annulus is

$$h_c = \frac{d_i Q}{\pi d_o L_e (T_{w,ave} - T_{c,ave})}, \quad (6)$$

where $T_{w,ave}$ is the wall average temperature summing all the thermocouples, $T_{c,ave}$ is the average temperature of the cooling water.

3.3 Pressure drop related to the R123 condensation heat transfer

For the horizontal two-phase flow, the total pressure drop includes the frictional component and the acceleration component,

$$\Delta P = \Delta P_f + \Delta P_a = P_{r,in} - P_{r,out}. \quad (7)$$

In which the acceleration pressure drop is computed based on the Tran correlation [11]:

$$\Delta P_a = G^2 \left[\frac{x^2}{\rho_v \alpha} + \frac{(1-x)^2}{\rho_l (1-\alpha)} \right]_{out} - G^2 \left[\frac{x^2}{\rho_v \alpha} + \frac{(1-x)^2}{\rho_l (1-\alpha)} \right]_{in}, \quad (8)$$

where G is the R123 mass flux. The void fraction α was estimated by the Smith equation [12]. ΔP_f was obtained by adjoining Eqs. (7) and (8).

3.4 Uncertainty analysis

High accuracy sensors and instruments were utilized for the experimental measurement. The Omega K-type thermocouples were used for temperature measurement with the uncertainty of 0.2 °C. The DMF-1-DX mass flow meters were used for mass flow rate measurement with the uncertainty of 0.1 %. The Rosemount-3051 pressure transducers were used for pressure measurement with the uncertainty of 1.0 %. In addition, the uncertainties of the voltage and current for the heating power computation were both 1.0 %.

The heat transfer coefficient, vapor quality and other parameters were determined by a set of measured parameters. We used the error transmission theory [13] to evaluate the uncertainties of these parameters. Thus, the condensation heat transfer coefficients had the maximum uncertainty of 12.6 %. The uncertainties of inlet and outlet vapor qualities had the accuracy of 1.5 % and 7.8 %, respectively.

4 Results and discussion

4.1 Test cases and flow observations

During the experiment, the temperature at helical-coiled tube inlet, the cooling water inlet temperature and the saturation pressure at test section inlet were maintained constant, covering the range of 10 ± 0.4 °C, 25 ± 0.3 °C, 250 ± 5 kPa. These parameters are seen in Table 1.

The high speed flow visualization was performed. The flow pattern map was plotted in a $J_g - X_{tt}$ coordinate (see Fig. 4). Three flow patterns are involved: annular flow, wavy-stratified flow and stratified flow. Among them, there are fewer cases for the stratified flow. The heat transfer performances related to the wavy-stratified flow and stratified flow are similar. Thus, the wavy-stratified flow and stratified flow are combined to be discussed. Besides, the obtained flow pattern map was compared with those provided for the horizontal pipe flow in Ref. [14]. They are generally matched with each other. In Fig. 4, the annular flow, stratified flow and the wavy-stratified flow were represented by A, SW and SS, respectively.

4.2 Heat transfer coefficients

Wall temperatures on the three specific locations over various cross sections directly indicate the heat transfer

Table 1 The major parameters and ranges

Parameters	Ranges
Mass flux of R123 flow (kg/(m^2 s))	100–500
Inlet temperature of the helical-coiled tube (°C)	10 ± 0.4
Inlet pressure of the test section (kPa)	250 ± 5
Inlet temperature of the test section (°C)	55 ± 0.5
Inlet vapor mass quality of the test section	0.042–0.934
Mass flow rates of the cooling water (kg/h)	300 ± 3, 500 ± 3, 700 ± 3
Inlet temperature of the cooling water (°C)	25 ± 0.3
Heat flux on the inner wall surface (kW/m^2)	12.79–66.20

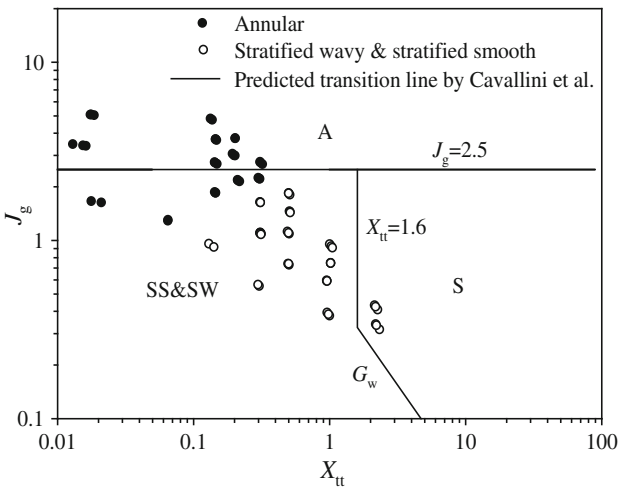

Fig. 4 The flow pattern map for the bare tube obtained in this study

performance. Figure 5 shows the wall temperatures for the bare tube (BT) and the micromembrance cylinder inserted tube (called MHTT) along the flow direction. The wall temperature on each cross section is averaged for the top, side and bottom wall locations. Figure 5a, b holds the annular flow pattern and the wavy-stratified flow patterns at the condenser inlet, respectively, having the positive vapor mass qualities at the condenser outlet, x_{out}. Figure 5c, d is for the wavy-stratified flow pattern at the condenser inlet, but having negative vapor mass qualities (subcooled liquid) at the condenser outlet. Generally, the MHTT increased the wall temperatures compared with the BT, depending on different cases. Figure 5a, b identified the increased wall temperatures by inserting the micromembrane cylinder for $x_{out} > 0$, indicating the heat transfer enhancement along the whole flow length. At the subcooled liquid outlet condition (see Fig. 5c), the wall temperatures are inter-crossed for the MHTT and BT along the flow direction. At the nearly saturated liquid inlet condition (see Fig. 5d), the MHTT increased the wall temperatures along the whole flow direction.

The heat transfer enhancement factor (EF) is defined as the heat transfer coefficients for the MHTT divided by those for the BT,

$$\mathrm{EF} = \frac{h_{\mathrm{MHTT}}}{h_{\mathrm{BT}}}. \tag{9}$$

Figure 6 shows EF values with R123 mass flux of 500 kg/(m^2 s) at various flow rates of the cooling water. Figure 6a illustrates both the MHTT and BT increased the condensation heat transfer coefficients with increases in the inlet vapor mass qualities, x_{in}. The lower flow rates of the cooling water increased the condensation heat transfer due to the large vapor mass qualities in the tube. The MHTT had larger condensation heat transfer coefficients than the BT. Figure 6b shows the EF values versus x_{in}. The maximum EF value reached 2.12, occurring at x_{in} of about 0.3. The minimum EF value takes place at $x_{out} \approx 0$

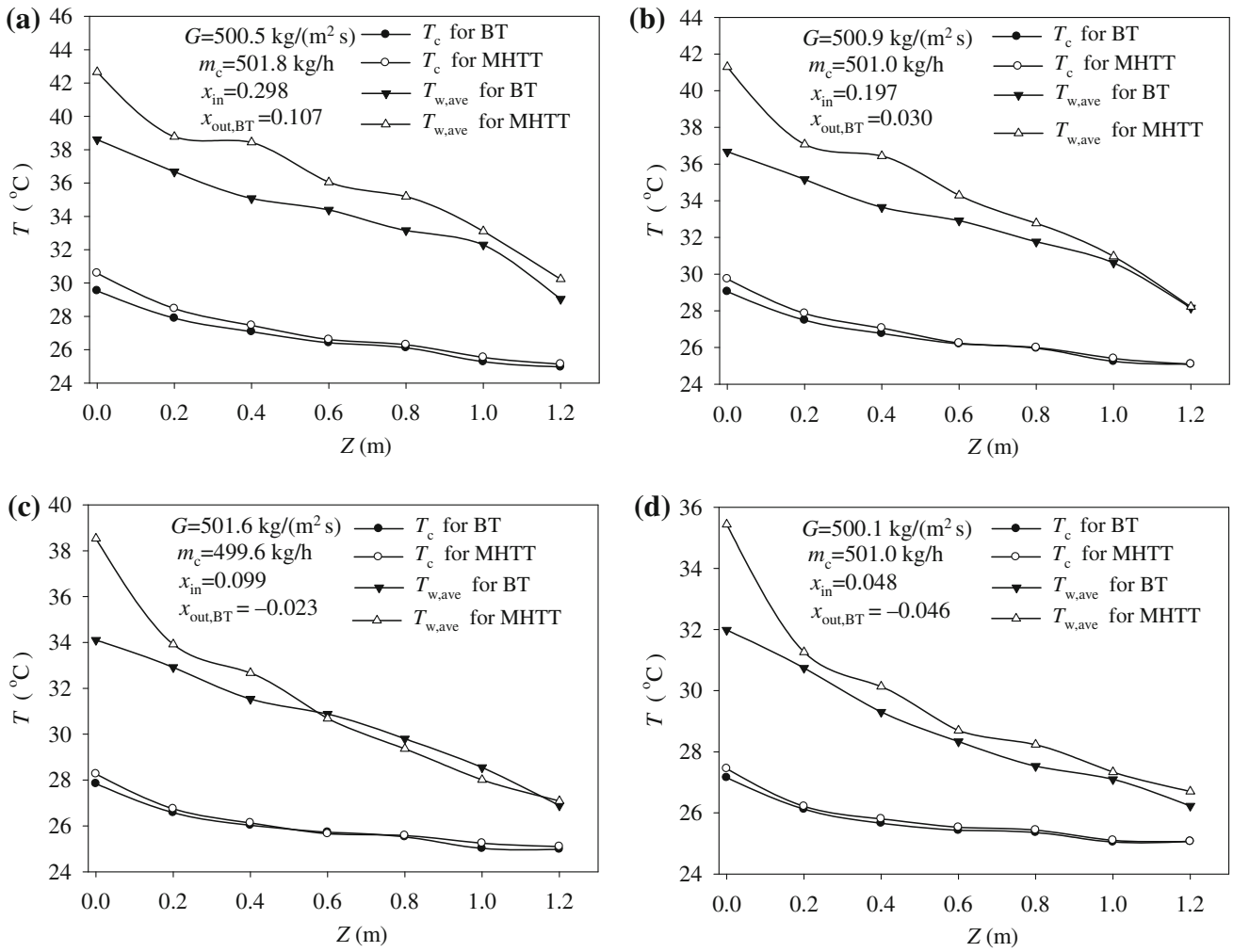

Fig. 5 The temperatures for the BT and MHTT along the flow direction

(near saturated liquid condition). At large inlet vapor mass quality, the EF values are smaller at larger flow rates of the cooling water. At smaller inlet vapor mass qualities, the EF values become larger at larger flow rates of the cooling water.

Other R123 mass fluxes show similar performance as those shown in Fig. 6. We note that the mass flux of the organic fluid is an important factor to influence the condensation heat transfer. Combining various factors, Fig. 7 summarizes the condensation heat transfer coefficients and heat transfer enhancement factors versus the vapor mass fluxes, i.e., Gx_{in}. Generally, the modulated heat transfer tube enhances heat transfer. Over the experimental data range, the heat transfer enhancement factors cover the range of 1.118–2.124. The heat transfer enhancement factors had minimum point against the vapor mass flux Gx_{in}. The cases before and after the minimum point occurring correspond to the subcooled outlet liquid condition and the two-phase outlet condition, respectively.

4.3 Pressure drop characteristics

Usually the heat transfer enhancement accompanies the penalty of the increased frictional pressure drop. Figure 8a shows the increased frictional pressure drops by inserting the micromembrane cylinder. The modulated heat transfer tube had stronger effect of the flow rates of the cooling water on the frictional pressure drop than the bare tube. The decrease of the flow rates of the cooling water increases the vapor mass qualities in the tube, resulting in the increased frictional pressure drop. To comprehensively evaluate the potential of micromembrane cylinder for low grade energy utilization, performance evaluation criterion

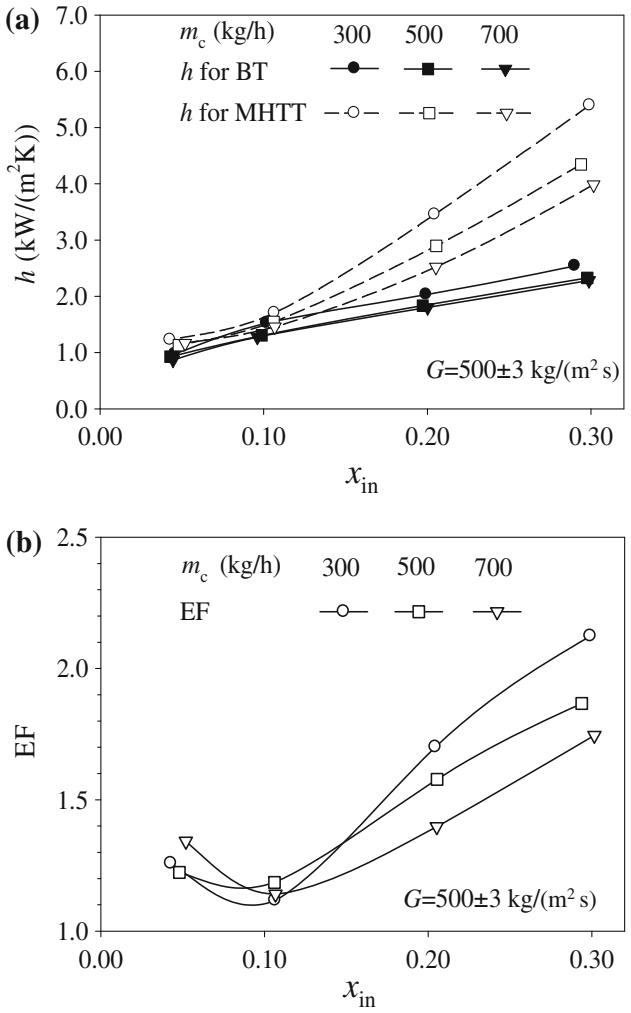

Fig. 6 The condensation heat transfer coefficients and transfer enhanced factors versus the vapor mass qualities at different flow rates of the cooling water

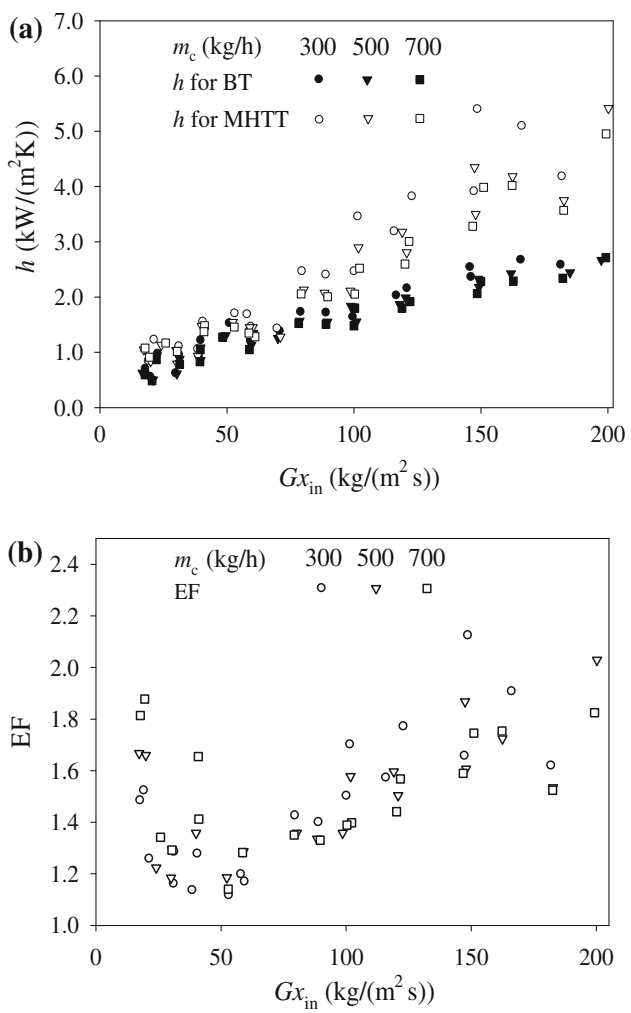

Fig. 7 The condensation heat transfer coefficients and transfer enhanced factors versus the vapor mass fluxes at different flow rates of the cooling water

(PEC) considering the quality of the thermal energy was chosen in this study. It was defined as [15, 16]:

$$\mathrm{PEC} = \frac{h_{\mathrm{MHTT}}/h_{\mathrm{BT}}}{\left(\Delta P_{\mathrm{f,MHTT}}/\Delta P_{\mathrm{f,BT}}\right)^{1/6}}. \quad (10)$$

Figure 8b shows the PEC values versus x_{in}, behaving the minimum points beyond which the PEC values are increased with x_{in} and decreased with the flow rates of the cooling water. Before the minimum point, the change trend of PEC against x_{in} and m_{c} are inverse to those after the minimum point.

Figure 8 illustrates the frictional pressure and PEC values at $G = 500$ kg/(m^2 s). Other mass fluxes show the similar trend as that presented in Fig. 8. Figure 9 summarizes all the data points of frictional pressure drop and PEC with Gx_{in} as the horizontal coordinate. The PEC curves also possess minimum points. The PEC values covered the range of 0.71–1.66, with most of runs behaving PEC larger than 1.0.

4.4 Heat transfer enhancement mechanism

The high speed flow visualization helps to clarify the heat transfer enhancement mechanisms. Figure 10 shows the flow images in the bare tube and the modulated heat transfer tube entrance at $G = 199$ kg/(m^2 s) and $x_{\mathrm{in}} = 0.103$. The bare tube had the stratified flow pattern with the liquid height of 7.13 mm. Inserting the micromembrane cylinder in the tube decreased the liquid height to 4.15 mm in the annular region. But the liquid height inside the micromembrane cylinder is higher than that in the bare tube. The surface tension force generated by the mesh pores held most of the liquid within the micromembrane cylinder, changing the phase distribution [17]. The modulated phase distribution over the tube cross section increased the contact vapor surface area with the tube wall, enhancing the condensation heat transfer. The increased friction drop is due to the increased vapor qualities or void fractions near the tube wall.

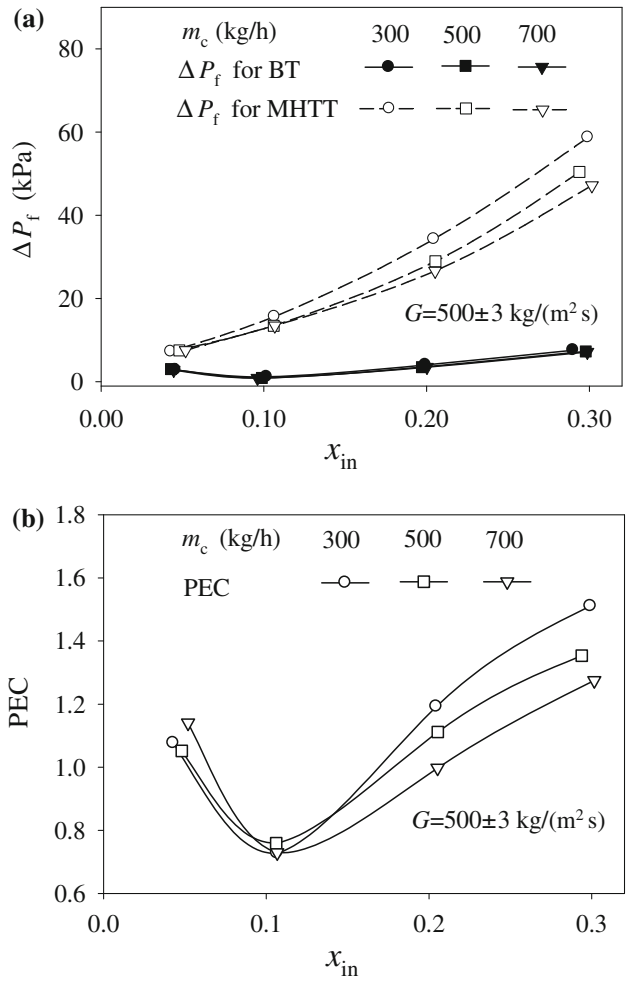

Fig. 8 The frictional pressure drop and PEC versus the inlet vapor mass quality x_{in}

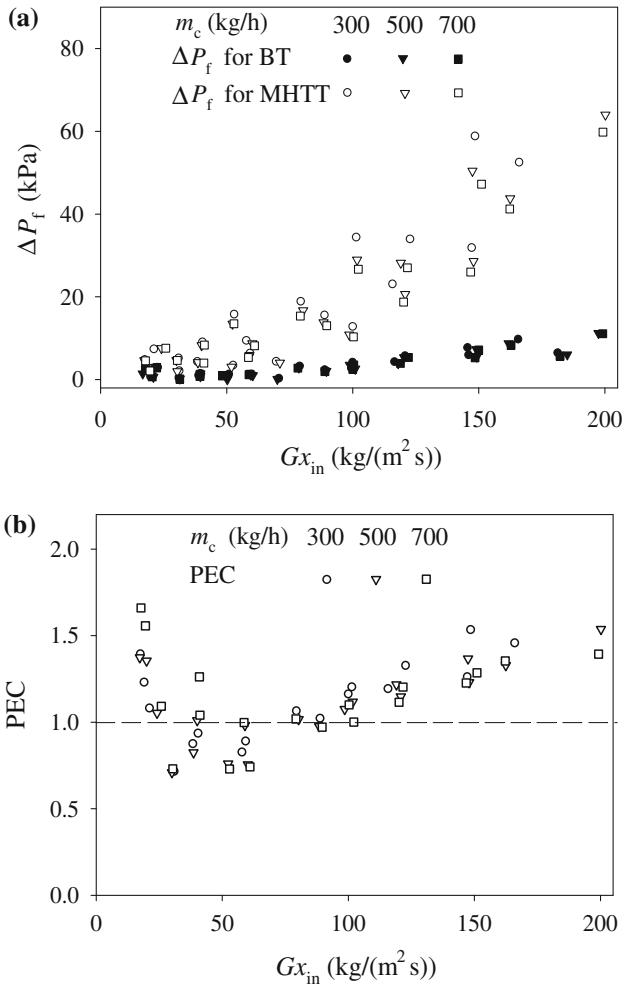

Fig. 9 The frictional pressure drop and PEC versus the inlet vapor mass flux Gx_{in}

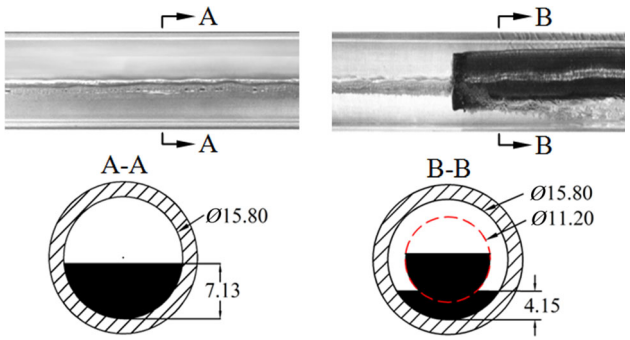

Fig. 10 (Color online) The flow image for the modulated stratified flow pattern

The modulation of the wavy-stratified flow pattern is similar to that shown in Fig. 10. It is difficult to identify how the two-phase mixture interacted with the micromembrane cylinder using the high speed camera only. The flow visualization in the microscale is necessary. The annular flow in the tube had the vapor core and liquid films on the tube wall. Miniature liquid droplets are entrained in the vapor core. Figure 11 shows the quick spreading process of the 1.25 mm diameter droplet of R123 liquid on the mesh screen surface. The mesh screen had PPI of 200 and the spreading process took place in millisecond timescale. This observation demonstrates the good wetting behavior of the mesh screen surface used in this study. When an annular flow stream interacts with the micromembrane surface, the entrained liquid droplets can be captured by the mesh pores surface. In other words, the micromembrane cylinder collected the droplets to enhance the vapor mass and volume content near the tube wall to enhance the condensation heat transfer.

In addition to the above physical process, the heat transfer performance is also related to the pressure drop and velocity variation along the flow direction. As shown in Fig. 12a, the inserted micromembrane cylinder divided the tube cross section into an annular region near the tube wall and a core region inside the micromembrane cylinder. The whole flow length may be subdivided into a two-phase part and a liquid flow part along the flow direction.

When a gas-liquid interface is involved near the mesh pores, the mesh pore induced surface tension force is written as

$$\Delta P_{\sigma} = \frac{4\sigma \cos\theta}{w}. \tag{11}$$

Such surface tension force resists the vapor phase entering the micromembrane cylinder inside. Small mesh pores generate apparently large surface tension. When the pressure difference across the two sides of the micromembrane cylinder, $P_{u,a} - P_{u,c}$, is smaller than ΔP_{σ}, the vapor phase will be maintained in the annular region near the tube wall. Liquid can be exchanged across the micromembrane surface, which can be estimated by the Darcy's law:

$$G_{leak} = (P_{u,a} - P_{u,c}) \times \frac{\rho}{\mu} \times \frac{k}{\delta}, \tag{12}$$

where ρ and μ are density and viscosity, k and δ are the micromembrane porosity and thickness.

The pressure analysis was performed here to consider the flow direction of the exchanged liquid mass. The two fluid streams from the core region and annular region are mixed at the tube exit. Thus, it is assumed $P_{e,a} = P_{e,c}$. Besides, the acceleration pressure drop is smaller and can be neglected compared with the frictional pressure drop. The pressure in the tube upstream (annular region) is written as

$$P_{u,a} = P_{e,a} + f_{SP,a} L_{SP} + f_{TP,a} \phi_{lo}^2 L_{TP}, \tag{13}$$

where $f_{SP,a}$ is the friction factor in the single-phase liquid flow length, $f_{TP,a}$ is the frictional factor assuming all the two-phase mixture flowing as liquid only, ϕ_{lo}^2 is the two-phase multiplier, L_{TP} and L_{SP} are the liquid flow length and two-phase flow length, respectively. The pressure in the tube upstream (core region) is expressed as

$$P_{u,c} = P_{e,c} + f_c \cdot (L_{SP} + L_{TP}), \tag{14}$$

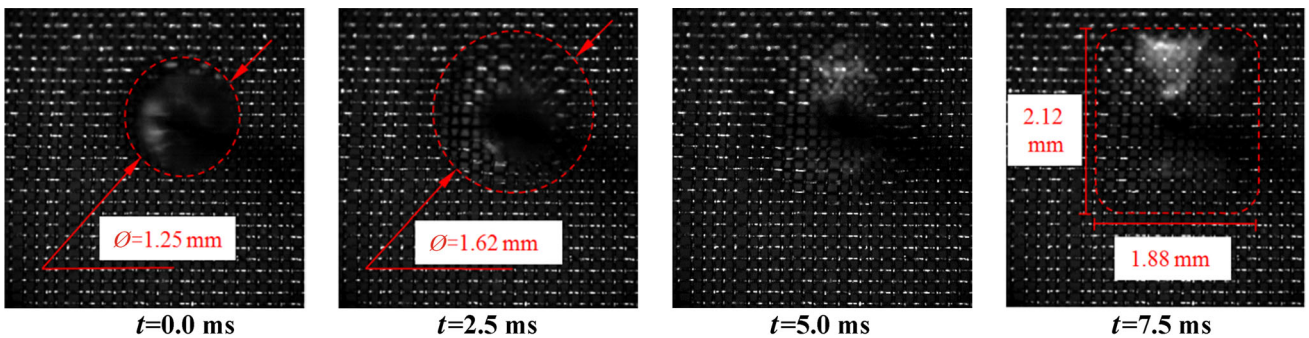

Fig. 11 (Color online) The high speed observation of a R123 liquid droplet spreading process on the mesh screen surface

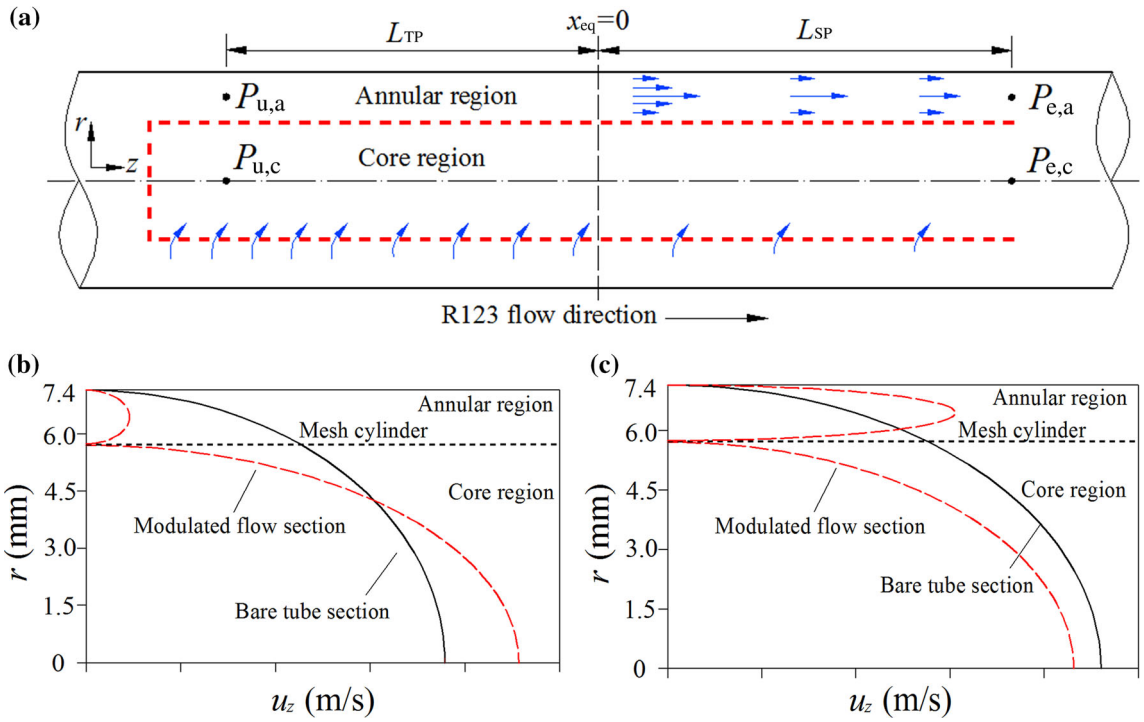

Fig. 12 (Color online) The pressure at various locations and the velocity distribution, **a** flow regions and pressures at different locations; **b** velocity distribution over the tube cross section for longer two-phase flow length; **c** velocity distribution over the tube cross section for short two-phase flow length

where f_c is the frictional factor of liquid flow in the core region.

Combining Eqs. (13) and (14) yields

$$P_{u,a} - P_{u,c} = (f_{SP,a} - f_{SP,c})L_{SP} + (f_{TP,a}\phi_{lo}^2 - f_{TP,c})L_{TP}, \quad (15)$$

ϕ_{lo}^2 is usually in the range of 10–100. Equation (15) gives the positive pressure difference from the annular region to the core region. That is, the pressure in the annular region is larger than the core region. The cases with $x_{out} > 0$ correspond to $L_{sp} = 0$ (see Fig. 5a, b), indicating the whole flow length covered by the two-phase mixture. The two-phase mixture was gradually condensed along the flow direction, and the condensed liquid flowed towards the core region. Thus, the void fractions near the tube wall are significantly larger than those for the bare tube to enhance the condensation heat transfer. Because ϕ_{lo}^2 is increased with increases in G and x_{in} to increase the frictional pressure drop, this increased the pressure difference from the annular region to the core region to enhance the liquid mass flow across the micromembrane surface, according to Eq. (12) and (15). This effect yields the condensation heat transfer enhancement more apparent.

The cases with $x_{out} < 0$ correspond to part of the flow length covered by two-phase mixture and single-phase liquid, respectively. The enhanced condensation heat transfer in the two-phase length obeys the same principle as that described as above. The heat transfer performance in the liquid flow length depends on the velocity distribution over the tube cross section. For a longer two-phase length (see Fig. 5c), much quantity of liquids flowed towards the core region to decrease the liquid flow rate in the annular region, having the decreased axial velocity near the tube wall as shown in Fig. 12b, under which the heat transfer in the liquid flow length is worsened.

The extremely low inlet vapor mass quality causes a short two-phase length (see Fig. 5d). Because the liquid mass flowing towards the core region is small due to the short two-phase length, the heat transfer in the whole flow length is similar to that for a single-phase liquid flow case. The limit case is $L_{TP} = 0$. Inserting micromembrane cylinder in a tube could enhance the forced convective liquid heat transfer [18]. Figure 12c shows the velocity distribution over the tube cross section to enhance the heat transfer.

5 Conclusions

The paper presented the preliminary experimental results for condensation in tube with micromembrane cylinder inserted. The effects of the structure parameters such as

PPI of micromembrane need specially investigated in the future. Major conclusions are summarized as follows.

(1) Inserting the micromembrane cylinder in a tube successfully modulates the flow patterns. The general trend is to force the vapor phase flowing in the annular region and liquid flowing in the core region. This increases the void fractions or vapor mass qualities near the wall to enhance the condensation heat transfer.
(2) The measured heat transfer enhancement factors cover the range of 1.18–2.12.
(3) The comprehensive performance evaluation criteria (PEC) had the range of 0.71–1.66, with most of runs behaving PEC larger than 1.0.
(4) The enhanced heat transfer mechanisms are analyzed with the observed images together with the discussion of pressure and velocity distributions.

Acknowledgements This work was supported by the National Natural Science Foundation of China of International Cooperation Project (51210011), the National Basic Research Program of China (2011CB710703), and the National Natural Science Foundation of China (U1034004).

References

1. Dewan A, Mahanta P, Raju KS et al (2004) Review of passive heat transfer augmentation techniques. Proc Inst Mech Eng A J Power 218:509–527
2. Han W, Sun L, Zheng D et al (2013) New hybrid absorption–compression refrigeration system based on cascade use of mid-temperature waste heat. Appl Energy 106:383–390
3. Kwon O, Cha D, Park C (2013) Performance evaluation of a two-stage compression heat pump system for district heating using waste energy. Energy 57:375–381
4. Graham D, Chato JC, Newell TA (1998) Heat transfer and pressure drop during condensation of refrigerant 134a in an axially grooved tube. Int J Heat Mass Transf 42:1935–1944
5. Cavallini A, Del Col D, Doretti L et al (2000) Heat transfer and pressure drop during condensation of refrigerants inside horizontal enhanced tubes. Int J Refrig 23:4–25
6. Miyara A, Otsubo Y (2002) Condensation heat transfer of herringbone micro fin tubes. Int J Therm Sci 41:639–645
7. Laohalertdecha S, Wongwises S (2011) Condensation heat transfer and flow characteristics of R-134a flowing through corrugated tubes. Int J Heat Mass Transf 54:2673–2682
8. Chen HX, Xu JL, Li ZJ et al (2012) Flow pattern modulation in a horizontal tube by the passive phase separation concept. Int J Multiph Flow 45:12–23
9. Sun DL, Xu JL, Chen QC et al (2013) Numerical study of flow pattern modulation in a vertical phase separation condenser tube. Chin Sci Bull 58:1592–1598
10. Laohalertdecha S, Wongwises S (2010) The effects of corrugation pitch on the condensation heat transfer coefficient and pressure drop of R-134a inside horizontal corrugated tube. Int J Heat Mass Transf 53:2924–2931
11. Tran TN (1998) Pressure drop and heat transfer study of two-phase flow in small channels. PhD dissertation, Texas Tech University, Texas
12. Smith SL (1969) Void fractions in two-phase flow: a correlation based upon an equal velocity head model. Proc Inst Mech Eng I J Syst 184:647
13. Abernethy RB, Thompson JW (1980) Handbook-uncertainty in gas turbine measurements. National Technical Information Service, Springfield
14. Cavallini A, Censi G, Del Col D, et al (2002) Intube condensation of halogenated refrigerants. Ashrae Trans, 108, Paper 4507
15. Zhang XY, Liu ZC, Liu W (2012) Numerical studies on heat transfer and flow characteristics for laminar flow in a tube with multiple regularly spaced twisted tapes. Int J Therm Sci 58:157–167
16. Fan JF, Ding WK, Zhang JF et al (2009) A performance evaluation plot of enhanced heat transfer techniques. Int J Heat Mass Transf 52:33–44
17. Chen HX, Xu JL, Li ZJ et al (2013) Stratified two-phase flow pattern modulation in a horizontal tube by the mesh pore cylinder surface. Appl Energy 112:183–1290
18. Cao Z, Xu J, Sun D et al (2014) Numerical simulation of modulated heat transfer tube in laminar flow regime. Int J Therm Sci 75:171–183